Nuclear Science and Techniques (2025) 36:213
https://doi.org/10.1007/s41365-025-01768-3

Enhanced suppression of background in capture reaction measurements with LAMBDA-II in ground laboratories

Lu-Yang Song[1] · Lin Wang[1] · Jun Su[1] · Li-Yong Zhang[1] · Jian-Jun He[1,2] · Shi-Lun Jin[3] · Fei Lu[4] · Yang-Ping Shen[5] · Jun-Feng Chen[6] · Yao-De Sheng[1] · Xin Chen[1] · Shen Lin[1] · Zhi-Wei Qin[1] · Zi-Ming Li[1] · Hao Zhang[1] · Luo-Huan Wang[1] · Yin-Ji Chen[1] · Xin-Zhi Jiang[1] · Zhi-Lin Shen[1] · Xin-Yue Li[1] · Feng-Cheng Liu[1] · Yi-Tong Huang[1] · Si-Ze Chen[7] · Bing Guo[5] · Wei-Ping Liu[5,8]

Received: 3 December 2024 / Revised: 17 March 2025 / Accepted: 25 March 2025 / Published online: 21 August 2025

Abstract

The precise determination of cross sections for key nuclear reactions within the Gamow window is crucial for advancing the study of stellar evolution and nucleosynthesis. However, extremely low reaction yields combined with the cosmic-ray-induced background make these measurements highly challenging, particularly for capture reactions. This work demonstrates the second configuration of the large-scale modular BGO detection array (LAMBDA-II) designed to capture reaction measurements and introduces a method for suppressing γ-ray detection background in ground laboratories. By employing active and passive shielding, the background of LAMBDA-II was significantly reduced by approximately two orders of magnitude, reaching 8.1×10^{-3} and 1.0×10^{-3} keV^{-1}h^{-1} in the 6–11 and 11–20 MeV energy ranges, respectively. When combined with a mA-scale intensity beam, this reduced background enables the investigation of several capture reactions of astrophysical interest in ground laboratories.

Keywords Nuclear astrophysics · Capture reaction · Background · Summing technique · γ detector array · Shielding

1 Introduction

Hydrostatic nuclear burning, which is the longest stage in a star's life, is driven by a series of light element fusion reactions. Among these, capture reactions are characterized by extremely small cross sections within the energy range of astrophysical interest (Gamow window), resulting in significant challenges for measurements [1, 2]. In

Supported by the National Key R&D Program of China (Nos. 2022YFA1602301, 2022YFA1603300, and 2023YFA1606701), National Natural Science Foundation of China (Nos. U1867211, 12275026, and 12222514), the CAS Light of West China Program grant No. 2020-82.

✉ Jun Su
sujun@bnu.edu.cn

✉ Li-Yong Zhang
liyongzhang@bnu.edu.cn

[1] Key Laboratory of Beam Technology of Ministry of Education, School of Physics and Astronomy, Beijing Normal University, Beijing 100875, China

[2] Key Laboratory of Nuclear Physics and Ion-beam Application (MoE), Institute of Modern Physics, Fudan University, Shanghai 200433, China

[3] Institute of Modern Physics, Chinese Academy of Sciences, Lanzhou 730000, China

[4] Shanghai Advanced Research Institute, Chinese Academy of Sciences, Shanghai 201210, China

[5] China Institute of Atomic Energy, P. O. Box 275(10), Beijing 102413, China

[6] Shanghai Institute of Ceramics, Chinese Academy of Sciences, Shanghai 201800, China

[7] Institute of Nuclear Energy Safety Technology, Hefei Institutes of Physical Science, Chinese Academy of Sciences, Hefei 230031, China

[8] Department of Physics, Southern University and Technology, Shenzhen 518005, China

addition, the cosmic-ray-induced background in ground laboratories further exacerbates these measurement challenges. Efforts to overcome these challenges have focused on enhancing beam intensity, increasing detection efficiency, and reducing background.

As the reaction yield scales with the beam intensity, increasing the beam intensity effectively improves the effect-to-background ratio in the measurements. Recently, mA-scale intensity proton beams have been achieved in several nuclear astrophysical facilities [3, 4], significantly enhancing the reaction yields but also posing challenges to the target stability [5, 6].

With a single high-purity germanium (HPGe) detector, the detection efficiency for γ rays in the MeV energy range emitted by capture reactions is low, usually on the order of a few percentages. The summing technique, which employs a scintillator detector array to achieve near 4π solid-angle coverage, significantly enhances the γ-ray detection efficiency [7, 8], advancing the measurement of capture reactions with low cross sections. Currently, several detector arrays are employed in nuclear astrophysical experiments, for instance, SuN [9] at the National Superconducting Cyclotron Laboratory (NSCL), HECTOR [10, 11] at the University of Notre Dame and the Compact Accelerator System for Performing Astrophysical Research (CASPAR), the BGO array [12] constructed in the Laboratory for Underground Nuclear Astrophysics (LUNA) at Laboratori Nazionali del Gran Sasso (LNGS), and the BGO array [13, 14] used in the Jinping Underground Nuclear Astrophysics experimental facility (JUNA) at China Jinping Underground Laboratory (CJPL).

Several methods can be used to reduce the background for γ-ray detection. Coincidence measurements such as γ–γ and charged particle–γ coincidences effectively reduce laboratory background [15–17], although they have specific limitations. For instance, the γ–γ coincidence method cannot be used to detect transitions in which a nucleus decays directly to its ground state by emitting only a single γ ray. In addition, the laboratory background can be significantly suppressed by compressing the beam into a short pulse [18]. The advantages of this method have been maximized in the study of laser-driven nuclear reactions with sub-nanosecond timescales [19, 20].

With the shielding provided by a kilometer-scale rock layer, underground laboratories can dramatically suppress the cosmic-ray-induced background, providing an ideal venue for nuclear astrophysical reaction studies. Currently, three underground nuclear astrophysics experimental facilities exist: LUNA [21] at INFN-LNGS, JUNA [22–24] at CJPL, and CASPAR [25] at SURF. Many experiments [11, 13, 26–33] focusing on the fusion reactions in hydrogen and helium burning have been performed in these underground facilities using the summing technique, providing a wealth of data for stellar evolution studies [34, 35].

Despite the significant advantages of underground experiments, many experiments [36–41] continue to be conducted in ground laboratories owing to the long measurement periods and limited beam times available in underground laboratories. Therefore, it is crucial to reduce the background of γ-ray detectors in ground laboratories. Recently, several studies have investigated the background of HPGe detectors using both active and passive shielding techniques [42–44]. Passive shielding effectively reduces the background from environmental radioactive nuclides, whereas active shielding significantly reduces the background induced by cosmic rays.

In this study, the second configuration of the large-scale modular BGO detection array (LAMBDA-II) was assembled specifically for nuclear astrophysics experiments. The laboratory background of LAMBDA-II was systematically measured under various shielding conditions. A significant reduction in the background, particularly within the energy ranges relevant to the capture reactions, was achieved using comprehensive shielding methods. Furthermore, the feasibility of using LAMBDA-II in conjunction with an mA-scale intensity beam to investigate capture reactions with low cross sections in ground laboratories was demonstrated by measuring the $^{15}N(p,\gamma)^{16}O$ reaction.

2 LAMBDA-II design

LAMBDA is a high-efficiency array primarily designed to measure the β-delayed γ decay of fission products [45]. It consists of 102 identical modules, each containing a 60 mm × 60 mm×120 mm bismuth germanate (BGO) crystal. Compared with other common scintillators, the BGO crystal, with an effective atomic number of 74.2 and a density of 7.13 g/cm^3, exhibits a higher detection efficiency for γ-rays. The excellent consistency in the efficiency and energy resolution of the LAMBDA modules [45] makes them highly suitable for summing techniques.

The rectangular design of the LAMBDA module allows flexible assembly into various configurations. To accommodate the nuclear astrophysical reaction measurements, 48 modules were configured in LAMBDA-II, as shown in Fig. 1. LAMBDA-II comprises two layers: an inner layer with 16 BGO modules (inner BGO modules) and an outer layer with 32 BGO modules (outer BGO modules). The center of LAMBDA-II features a 64 mm × 64 mm square hole for positioning the reaction target and vacuum pipe. LAMBDA-II operates in two modes based on the laboratory background levels. In underground laboratories with a minimal background, both the inner and outer BGO modules

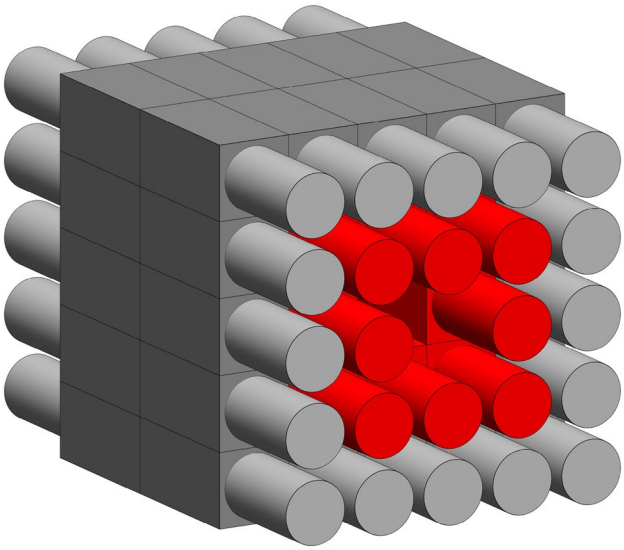

Fig. 1 Schematic of the LAMBDA-II structure. LAMBDA-II consists of 48 modules: the inner and outer BGO modules are shown in red and gray, respectively

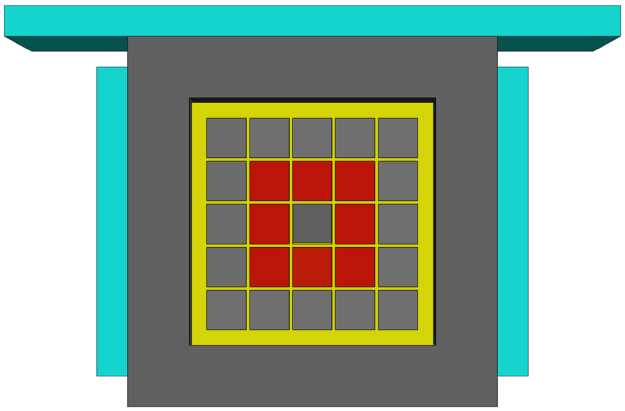

Fig. 2 Schematic of the LAMBDA-II shielding system. From inside to outside, the materials include: inner BGO modules (red), outer BGO modules (gray), BCH frame (yellow), a 10-cm-thick Pb layer (deep gray), and a 5-cm-thick plastic scintillator detectors (cyan)

are used to construct the sum spectra, maximizing the γ-ray detection efficiency. Conversely, in ground laboratories with high background levels, the inner BGO modules function as primary detectors, whereas the outer BGO modules serve as anti-coincidence detectors to generate veto signals for background reduction.

The average energy resolution of LAMBDA-II was measured as 10.0% using a ^{137}Cs source. A simulation with GEANT4 [46] showed that the summing efficiencies of all BGO modules exceed 75% in the 1–10 MeV energy range when the source is positioned at the center of LAMBDA-II and the center hole remains empty. Compared to HECTOR and SuN, which are commonly used for measuring capture reactions in ground laboratories, the energy resolution of LAMBDA-II is slightly inferior, but its detection efficiency is higher. Taking advantage of these high efficiencies, the use of LAMBDA-II is expected to significantly enhance the precision of capture reaction measurements at the JUNA facility.

At typical γ-ray energies (6–20 MeV) relevant to capture reactions, the laboratory background mainly originates from secondary particles induced by cosmic rays, such as muons, pions, γ rays, electrons, protons, and neutrons [43]. Accordingly, a shielding system was designed for LAMBDA-II to reduce the laboratory background, as shown in Fig. 2. The LAMBDA-II modules were embedded within a grid frame made of 20% borated polyethylene (BCH), which effectively moderates and absorbs neutrons. The outer layer of the BCH frame is 2.5 cm thick, with internal partitions measuring 0.5 cm in thickness. Surrounding this frame, a 10-cm-thick lead (Pb) layer provides 4π shielding to absorb γ-rays. Finally, 5-cm-thick plastic scintillator detectors were positioned on the outermost layer, except at the bottom, to veto muon signals, as muons primarily originate from above the detector.

3 Background measurement and analysis

The background measurements of LAMBDA-II were conducted in a ground laboratory at Beijing Normal University (BNU). The signals were recorded using a data acquisition system based on Pixie-16 modules from XIA LLC [47], with a sampling frequency of 100 MHz and a resolution of 14 bits. Energy and time stamp data were recorded for both the BGO modules and plastic scintillator detectors. During the experimental data analysis, the γ-ray energy spectra of each BGO module were calibrated using the 1461 and 2614 keV peaks from ^{40}K and ^{208}Tl decays. After calibration, the summing spectrum (E_{sum}) was obtained by summing the energies recorded by the inner BGO modules with a $\pm$800 ns coincidence time window. Additionally, the sum of the energies recorded by the outer BGO modules was used as the BGO veto signal (V_{BGO}), whereas the sum of the energies from the plastic scintillator detectors served as the plastic scintillator veto signal (V_{plastic}).

To investigate the effects of various shielding measures, the laboratory background of LAMBDA-II was measured under a series of incremental shielding conditions:

(1) Without any shielding.
(2) With 10 cm Pb shielding.
(3) With 10 cm Pb shielding and plastic scintillator detectors.
(4) With 10 cm Pb shielding and 25 cm BCH shielding.

(5) With 10 cm Pb shielding, plastic scintillator detectors, and 1 mm cadmium shielding.
(6) With a BCH frame, 10 cm Pb shielding, and plastic scintillator detectors.

Figure 3 shows a comparison of the background measured without any shielding and with 10 cm Pb shielding. It is clear that the reduction in background varied significantly across the different energy regions. At energies below 3 MeV, the background is primarily produced by natural radioactivity. Above 3 MeV, the background is mainly caused by secondary particles induced by cosmic rays [43]. In the energy range 0.5 MeV $< E_{sum} <$ 3 MeV, the background was reduced by approximately one order of magnitude. This reduction is particularly evident from the representative 1461 and 2614 keV peaks from ^{40}K and ^{208}Tl decays, which were effectively absorbed by the 10 cm Pb layer. However, the intrinsic background, such as the 940 and 1633 keV peaks originating from the α particles emitted by ^{210}Po decay and the 1063–570 keV cascade γ-rays from ^{207}Bi decay, remained unaffected. For the energy range 3 MeV $< E_{sum} <$ 50 MeV, only a minor reduction factor of approximately 2 was observed. The background in this energy range is believed to have a complex origin, primarily originating from various secondary particles induced by cosmic rays that are not effectively absorbed by the Pb layer. At energies above 50 MeV, no significant reduction in the background energy was observed, indicating that the main contributors were high-energy muons, which could easily pass through the Pb layer.

To further suppress the cosmic-ray-induced background, which cannot be effectively reduced by Pb shielding alone, an anti-coincidence technique was adopted by introducing plastic scintillator detectors. In addition, the outer BGO modules of LAMBDA-II were employed as veto detectors. An anti-coincidence time window of ±800 ns was applied. Based on the 10 cm Pb shielding, Fig. 4 compares the background obtained without any veto, with V_{BGO}, with $V_{plastic}$, and with $V_{BGO} + V_{plastic}$. It is evident that anti-coincidence significantly reduces the background across the full energy region, with more pronounced effects at higher E_{sum} energies. In addition, V_{BGO} provides stronger suppression of the background than $V_{plastic}$, indicating that the outer BGO modules have a higher detection efficiency for cosmic-ray-induced particles. However, the outer BGO modules did not cover the inner BGO modules along the axial direction, limiting their ability to veto cosmic-ray-induced particles entering at low horizontal angles. Therefore, the background was further reduced when both V_{BGO} and $V_{plastic}$ were combined in an anti-coincidence manner, as shown in Fig. 4.

The reduction in background after anti-coincidence varied across different energy ranges. In the 50–200 MeV energy range, the background was reduced by a factor of approximately 500, indicating that the contribution from muons was dramatically suppressed. In the 6–50 MeV energy range, a lower reduction factor of approximately 25 was observed, suggesting that part of the background could not be effectively removed using the anti-coincidence method. Notably, three characteristic peaks at approximately 6.8, 7.4, and 10.2 MeV were observed after anti-coincidence. These peaks are supposed to be caused by the thermal neutron

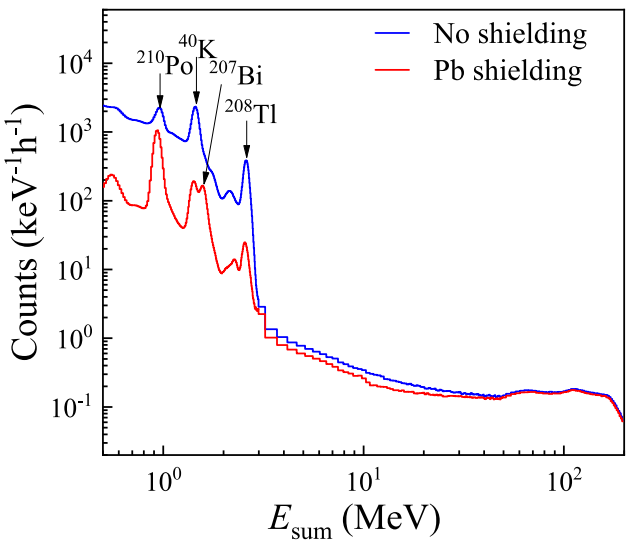

Fig. 3 Background measured with (red line) and without (blue line) 10 cm Pb shielding. The peaks from radioactive nuclide decays are marked

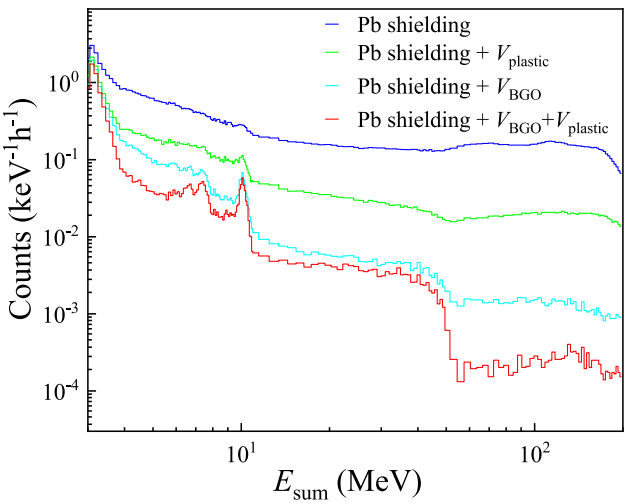

Fig. 4 Background measured with 10 cm Pb shielding and various anti-coincidence methods, including no veto (blue line), plastic scintillator veto (green line), outer BGO modules veto (cyan line), and the combined veto of plastic scintillator detectors and outer BGO modules (red line)

capture on germanium (Ge) isotopes, as the peak energies correspond to the Q-values of the ^{70}Ge$(n,\gamma)^{71}$Ge (7.4 MeV), ^{72}Ge$(n,\gamma)^{73}$*Ge* (6.8 MeV), and ^{73}Ge$(n,\gamma)^{74}$*Ge* (10.2 MeV) reactions. Additionally, the ratio of the areas of these peaks is consistent with that of the reaction yields calculated using the thermal neutron capture cross sections and Ge isotope abundances.

To confirm that the characteristic γ-ray peaks originated from neutron capture reactions on the Ge isotopes, LAMBDA-II was wrapped in a 1-mm-thick Cd layer with additional 1-mm-thick Cd pieces inserted into the gaps between the BGO modules. As shown in Fig. 5, the γ-ray peaks attributed to neutron capture on the Ge isotopes were significantly reduced by adding the Cd material, whereas a new characteristic γ-ray peak appeared at approximately 9.0 MeV. The energy of this new peak was consistent with the Q value of the ^{113}Cd$(n,\gamma)^{114}$Cd reaction, which confirms that some neutrons were captured by the Cd layer. In addition, the summing spectrum of the inner BGO modules resulting from the Ge(n,γ) capture reactions was simulated using GEANT4 with its built-in physics list (named FTFP_BERT_HP), which reproduces the three measured peaks well, as shown in Fig. 5.

To explore the origin of the thermal neutrons captured by the Ge isotopes, an additional 25-cm-thick 20% BCH layer was externally added and placed on all six sides of the Pb shielding. As the size of the BCH blocks was not sufficient to fully cover the plastic scintillator detectors, they were removed during this measurement. A previous study showed that a 22.4-cm-thick 5% BCH layer can absorb approximately 98% of the neutrons emitted by Am-Be and ^{252}Cf sources [48]. Therefore, if neutrons come from outside the Pb layer, they would be predominantly absorbed by the BCH layer, resulting in the disappearance of the three characteristic peaks associated with thermal neutron capture. However, as shown in Fig. 6, these peaks were only partially suppressed after the addition of BCH shielding. This observation indicates that a fraction of the neutrons did not originate from the external environment, but were produced within materials located inside the BCH shielding, including the Pb layer and LAMBDA-II itself.

Neutron emission within the Pb shielding and BGO crystals can arise either from intrinsic radioactivity or from interactions induced by external radiation. The former can be excluded because no significant neutron capture peaks were observed in the background when measured for the BGO detector with Pb shielding in an underground laboratory [49]. For the latter, secondary cosmic rays, such as muons, can produce neutrons when interacting with Pb and BGO materials [50]. These high-energy radiations can easily penetrate the BCH shielding. If neutron capture reactions are prompt, they should be effectively vetoed by using plastic scintillator detectors. However, as shown in Fig. 4, the reduction in the neutron capture peaks in the background when V_{BGO} was applied remained minimal. This suggests that neutron capture reactions occur as delayed events relative to the precursor particles and therefore cannot be completely excluded by the ±800 ns anti-coincidence time window.

To validate this hypothesis, a microsecond-scale correlation analysis between the signals from the inner BGO modules and the preceding adjacent signals from the plastic scintillator detectors was performed on the measured data, as shown in Fig. 4. The observed time difference (ΔT)

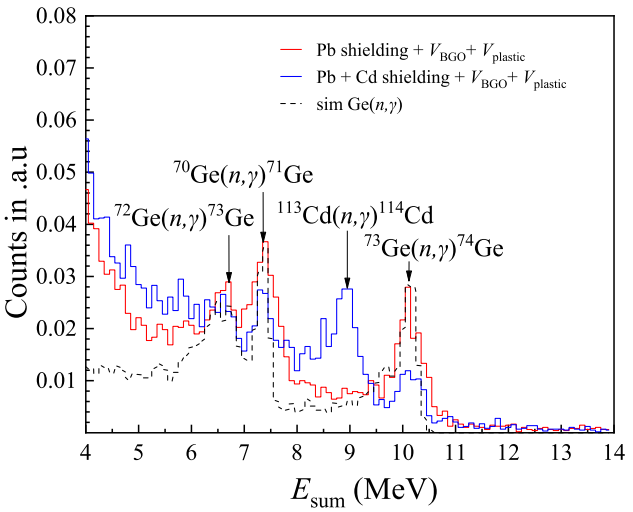

Fig. 5 Comparison of the background obtained with (blue line) and without (red line) 1 mm Cd shielding; both configurations include the vetoes of the outer BGO modules and plastic scintillator detectors. The black dashed line represents the simulated summing spectrum resulting from Ge(n,γ) reactions

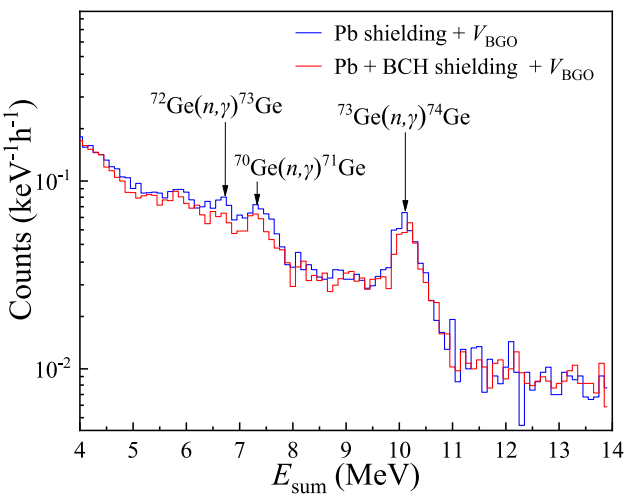

Fig. 6 Background obtained with (red line) and without (blue line) 25 cm BCH shielding, both are with the outer BGO modules veto

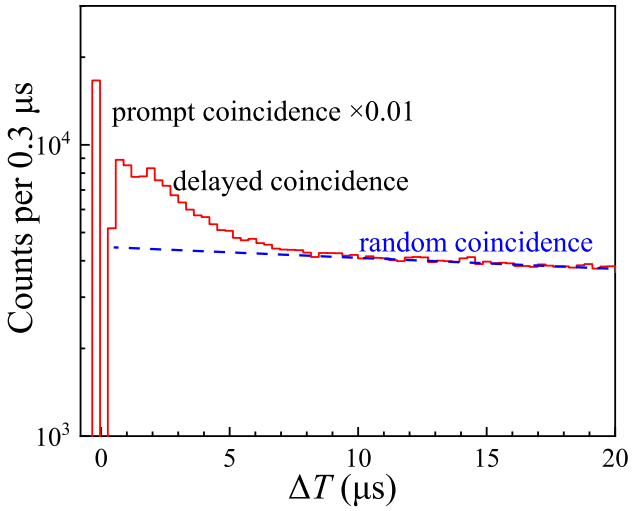

Fig. 7 Histogram of the time difference between the signal from the inner BGO modules and the previous adjacent signal from the plastic scintillator detectors. The blue dashed line represents the fit to the data for $\Delta T > 10$ μs based on an exponential decay trend

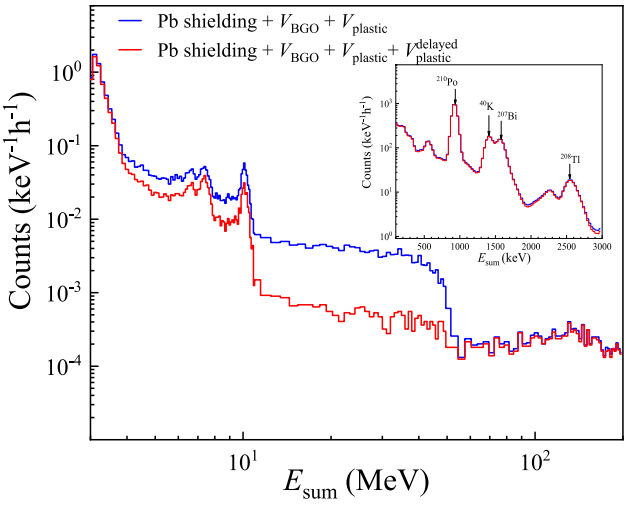

Fig. 8 Comparison of the background obtained with (red line) and without (blue line) $V_{plastic}^{delayed}$. Both are with the Pb shielding and $V_{BGO} + V_{plastic}$. The inset illustrates the background at low energies

spectra are shown in Fig. 7, which reveal three distinct time distribution structures. The front-most peak, scaled down by a factor of 0.01 for better visualization, corresponds to prompt coincidences. Events with $\Delta T > 10$ μs exhibit an exponential decay pattern, which is consistent with the time difference distribution of two adjacent accidental coincidence events. However, in the range 1 μs$< \Delta T < 10$ μs, a significant excess beyond the exponential decay trend was observed. This finding supports the hypothesis that delayed events contribute to part of the background.

To further suppress the background produced by the delayed events, an additional delayed veto signal ($V_{plastic}^{delayed}$) was introduced, which was used to reject events occurring within 10 μs after each trigger from the plastic scintillator detectors. As shown in Fig. 8, this delayed anti-coincidence significantly reduced the background in the 6–50 MeV energy range. Notably, a reduction by a factor of approximately 8 was observed in the 11–50 MeV plateau, which exhibited a strong correlation with delayed events. It is hypothesized that this plateau is caused by energy deposition in the BGO crystals owing to neutron moderation. For the neutron capture peaks, the reduction effect is present but is much smaller, which is consistent with the conclusion that some neutrons originate from outside the Pb shielding. In addition, this delayed veto has a negligible impact on the background above 50 MeV.

While further reducing the background, $V_{plastic}^{delayed}$, combined with the ~ 5 k count rate of the plastic scintillator detectors, results in a ~ 5% reduction in effective nuclear reaction events owing to random coincidence. This reduction estimate was confirmed by comparing the counts of the 940 keV peak with and without the delayed veto, as shown in the inset of Fig. 8. This peak is attributed to the α decay of the intrinsic ^{210}Po impurities within the BGO crystal. These α particles cannot penetrate the BGO crystal to reach the plastic scintillator detectors and can only be vetoed through random coincidence.

As shown in Fig. 8, the background level in the 6–11 MeV range, which is of particular importance for capture reaction measurements, remained significantly higher than that above 11 MeV, even after applying the delayed veto. This persistent background is attributed to two factors: (1) the absence of a 25-cm-thick BCH shielding outside the Pb shielding, as its dimensions are inadequate to fully cover the plastic scintillator detectors, and (2) the limitation of the width of the delayed veto time window owing to its impact on the dead time of nuclear reaction measurements. Therefore, a practical solution is required to effectively absorb neutrons and reduce the background caused by neutron capture reactions.

Adding a Cd layer can effectively absorb thermal neutrons but introduces a new γ peak at 9.0 MeV, as shown in Fig. 5. BCH is a good alternative to Cd because the ^{10}B(n, $\alpha\,\gamma$)^{7}Li reaction produces only a 478 keV γ-ray, which has no impact on the capture reaction measurements. A grid frame composed of BCH was constructed, and the LAMBDA-II modules were embedded within it, as shown in Fig. 2. As presented in Fig. 9, the γ-ray peaks caused by neutron capture on Ge isotopes were significantly suppressed by the BCH frame, leading to a substantially lower background in the 6–11 MeV range. However, a slight increase in the background was observed in other energy regions. This increase was attributed to the larger gaps introduced between the BGO modules by the BCH frame, which reduced the veto efficiency of the outer BGO

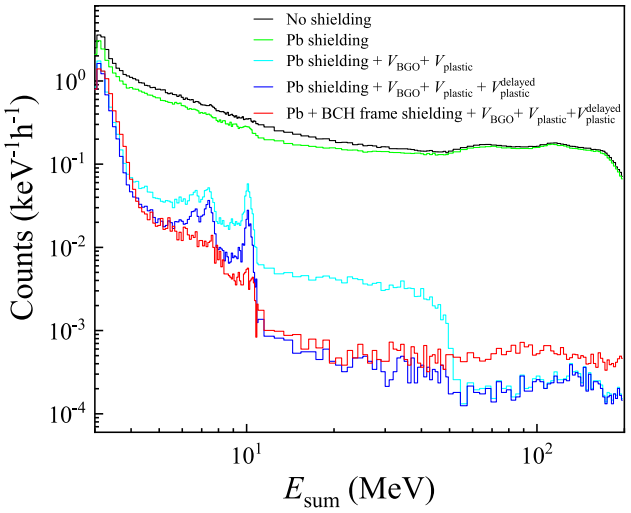

Fig. 9 Comparison of the background obtained under different shielding measures implemented in this work, as well as that without shielding

modules. In addition, the use of the BCH frame decreased the summing efficiency of LAMBDA-II, as shown in Fig. 10.

Figure 9 also compares the background obtained under different shielding measures implemented in this work, as well as that without shielding. For the 6–20 MeV energy range, the background was significantly reduced by the combined use of passive and active shielding measures. The Pb shielding mainly absorbed the γ-rays from the laboratory environment. $V_{BGO} + V_{plastic}$ effectively suppressed the prompt signals caused by the secondary cosmic rays interacting with the inner BGO modules. $V^{delayed}_{plastic}$ further reduced the delayed responses induced by neutrons generated from secondary cosmic rays interacting with the Pb and BGO materials. Finally, the BCH frame absorbed neutrons from various sources, effectively suppressing the neutron capture γ-ray peaks. However, as shown in Fig. 9, after various shielding measures, the background below 11 MeV remained relatively high, significantly exceeding that above 11 MeV, which requires further investigation.

The specific background levels under various shielding conditions are summarized in Table 1. The optimized background levels in the 6–11 MeV and 11–20 MeV energy ranges are 8.1×10^{-3} keV^{-1}h^{-1} and 1.0×10^{-3} keV^{-1}h^{-1}, respectively. These background levels were approximately two orders of magnitude higher than those observed for BGO detector arrays in underground laboratories [13, 51].

The detection efficiency of LAMBDA-II decreased with the addition of the BCH frame. This is partly due to the increased distance between the BGO modules and partly

Table 1 Comparison of the background levels (keV^{-1}h^{-1}) under different shielding conditions, as well as that without shielding

Shielding conditions	6–11 MeV	11–20 MeV
No shielding	4.4×10^{-1}	2.4×10^{-1}
Pb shielding	3.4×10^{-1}	1.8×10^{-1}
Pb shielding + V_{BGO}+$V_{plastic}$	3.0×10^{-2}	4.8×10^{-3}
Pb shielding+ V_{BGO}+$V_{plastic}$ + $V^{delayed}_{plastic}$	1.7×10^{-2}	8.2×10^{-4}
Pb + BCH frame shielding + V_{BGO} +$V_{plastic}$ + $V^{delayed}_{plastic}$	8.1×10^{-3}	1.0×10^{-3}

because the BCH frame absorbs some of the gamma-ray energy. Figure 10 presents a comparison of the detection efficiency of LAMBDA-II with and without the BCH frame based on Geant4 simulations. To reduce the background, the detection efficiency of LAMBDA-II used in the ground laboratory (green line in Fig. 10) is approximately 30% lower than that used in an underground laboratory (red line in Fig. 10). This decrease in detection efficiency would hinder the capture reaction measurements.

4 In-beam commissioning of LAMBDA-II in a ground laboratory

To evaluate the ability of LAMBDA-II to measure astrophysical capture reactions in ground laboratories, in-beam commissioning was performed by measuring the γ-rays emitted from the $^{15}N(p,\gamma)^{16}O$ reaction. This reaction represents the

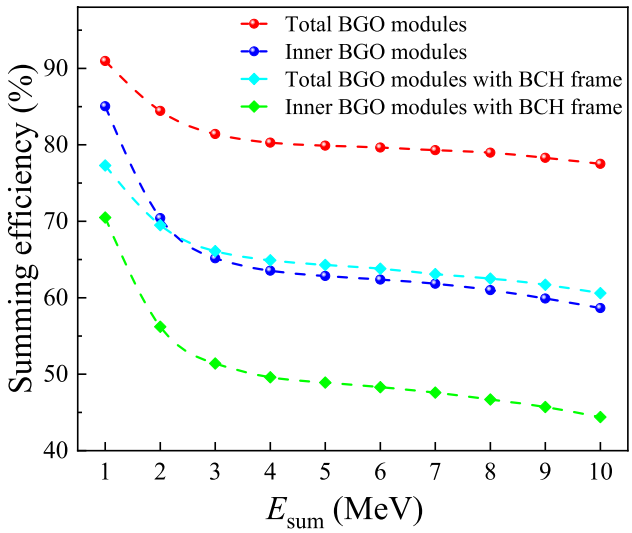

Fig. 10 Summing efficiencies of LAMBDA-II obtained by Monte Carlo simulations. Red and blue dots represent the summing efficiencies of the total BGO modules and the inner BGO modules, respectively. Cyan and green diamonds indicate the summing efficiencies of the total modules and inner BGO modules, respectively, when LAMBDA-II is positioned within the BCH grid frame

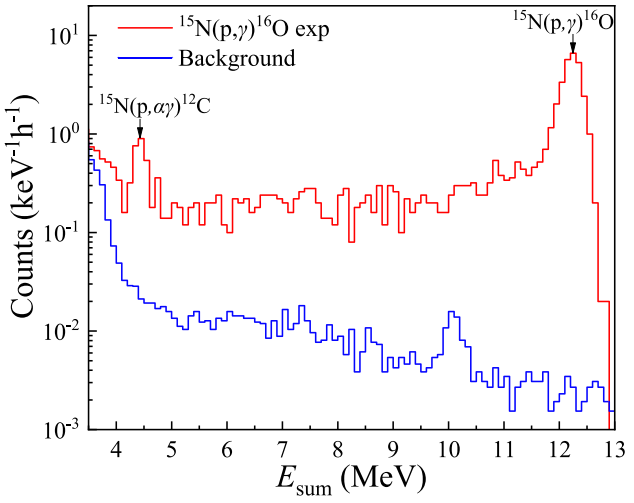

Fig. 11 Comparison between the summing spectrum (red line) obtained at $E_p = 125$ keV for the $^{15}N(p,\gamma)^{16}O$ reaction and the suppressed laboratory background (blue line). The origins of the γ-ray peaks are marked on the spectrum for clarity

first branching point in the carbon–nitrogen–oxygen (CNO) cycle and plays an important role in hydrogen burning in massive stars [2]. The reaction rate ratio of $^{15}N(p,\gamma)^{16}O$ to $^{15}N(p,\alpha)^{12}C$ governs the abundance of C, N, and O during early stellar evolution, directly influencing nucleosynthesis in later stages. Several studies [52–55] have directly measured the cross sections of the $^{15}N(p,\gamma)^{16}O$ reaction. The lowest energy point, $E_p = 74$ keV, was achieved by Caciolli et al. [56] in the LUNA underground laboratory. However, systematic discrepancies in the results reported in previous studies remain unresolved, necessitating further investigation.

In this experiment, LAMBDA-II and its shielding system were installed at the 350 kV accelerator located at the Institute of Nuclear Energy Safety Technology (INEST) of the Chinese Academy of Sciences [4]. The proton beam was collimated and directed onto a Ti^{15}N target positioned at the center of LAMBDA-II. The typical beam current applied to the target was approximately 2 mA. Figure 11 shows the E_{sum} spectrum obtained at $E_p = 125$ keV, where the sum peak at approximately 12.2 MeV caused by the $^{15}N(p,\gamma)^{16}O$ reaction is clearly visible. For comparison, the laboratory background measured for LAMBDA-II at INEST is shown in Fig. 11. This background level is slightly higher than that measured at BNU, primarily because of the 7-cm-diameter aperture in the Pb shielding to accommodate the vacuum pipe for beam transport, which prevents full spatial coverage.

Under the sum peak of the $^{15}N(p,\gamma)^{16}O$ reactions, as shown in Fig. 11, the background counting rate is approximately three counts per hour, which is only approximately one-thousandth of the measured effective counting rate. Using the S-factors provided by NACRE II [57], the capability of LAMBDA-II to measure the cross sections of the $^{15}N(p,\gamma)^{16}O$ reaction at lower energies was evaluated by assuming a constant beam intensity of 2 mA on the target and ensuring a signal-to-background ratio above 1:1. The results indicate that this low background level allows for the measurement of the $^{15}N(p,\gamma)^{16}O$ reaction down to $E_p = 62$ keV, which is 12 keV lower than the lowest energy point previously achieved [56].

5 Summary

In this study, LAMBDA-II was developed to measure the capture reactions of astrophysical interest. Its two-layer structure makes it suitable for experiments conducted in both underground and ground laboratories. The high detection efficiency of LAMBDA-II is expected to significantly enhance the precision of future experiments conducted at the JUNA facility. The origin of the background of LAMBDA-II in the ground laboratories was systematically investigated through measurements under a series of incremental shielding conditions. By combining Pb and BCH frame shielding, vetoes from the plastic scintillator detectors and outer BGO modules, and delayed vetoes, the background was significantly reduced to $8.1 \times -3\,\mathrm{keV^{-1}h^{-1}}$ and $1.0 \times -3\,\mathrm{keV^{-1}h^{-1}}$ in the 6–11 and 11–20 MeV ranges, respectively. The capability of LAMBDA-II to measure astrophysical capture reactions in ground laboratories was demonstrated by measuring $^{15}N(p,\gamma)^{16}O$ reactions.

Author contributions All authors contributed to the study conception and design. LAMBDA-II and its shielding system were designed by Lu-Yang Song, Jun Su, and Li-Yong Zhang. The experiment was carried out by Lu-Yang Song, Lin Wang, Yao-De Sheng, Xin Chen, Shen Lin, Zhi-Wei Qin, Zi-Ming Li, Hao Zhang, Luo-Huan Wang, Yin-Ji Chen, Xin-Zhi Jiang, Zhi-Lin Shen, Xin-Yue Li, Feng-Cheng Liu, and Yi-Tong Huang. Data analy sis was performed by Lu-Yang Song and Lin Wang. Chen Jun-Feng, Shi-Lun Jun, Fei Lu, and Yang-Ping Shen provided BGO materials for the construction of LAMBDA-II. Si-Ze Chen provided the experimental platform for the in-beam commissioning. The first draft of the manuscript was written by Lu-Yang Song, and all authors commented on previous versions of the manuscript. All authors read and approved the final manuscript.

Data availability The data that support the findings of this study are openly available in Science Data Bank at https://cstr.cn/31253.11.sciencedb.j00186.00727 and https://doi.org/10.57760/sciencedb.j00186.00727.

Declarations

Conflict of interest The authors declare that they have no competing interests.

References

1. C.E. Rolfs, W.S. Rodney, *Cauldrons in the cosmos: nuclear astrophysics* (University of Chicago Press, 1988)
2. C. Iliadis, *Nuclear physics of stars* (John Wiley & Sons, 2015)
3. Q. Wu, L.T. Sun, B.Q. Cui et al., Design of an intense ion source and LEBT for Jinping underground nuclear astrophysics experiments. Nucl. Instrum. Methods Phys. Res., Sect. A **830**, 214–218 (2016). https://doi.org/10.1016/j.nima.2016.05.099
4. Y.J. Chen, L.Y. Zhang, S.Z. Chen et al., A new platform for nuclear astrophysics studies on Hefei Facility. Nucl. Instrum. Methods Phys. Res., Sect. B **1054**, 168401 (2023). https://doi.org/10.1016/j.nima.2023.168401
5. L.Y. Zhang, Y.J. Chen, J.J. He et al., Strong and durable fluorine-implanted targets developed for deep underground nuclear astrophysical experiments. Nucl. Instrum. Methods Phys. Res., Sect. B **496**, 9–15 (2021). https://doi.org/10.1016/j.nimb.2021.03.017
6. L.H. Wang, Y.P. Shen, J. Su et al., Development of irradiation-resistant enriched ^{12}C targets for astrophysical $^{12}C(\alpha,\gamma)^{16}O$ reaction measurements. Nucl. Instrum. Methods Phys. Res., Sect. B **512**, 49–53 (2021). https://doi.org/10.1016/j.nimb.2021.11.020
7. P. Tsagari, M. Kokkoris, E. Skreti et al., Cross section measurements of the $^{89}Y(p,\gamma)^{90}Zr$ reaction at energies relevant to*p*-process nucleosynthesis. Phys. Rev. C **70**, 015802 (2004). https://doi.org/10.1103/PhysRevC.70.015802
8. A. Spyrou, H.-W. Becker, A. Lagoyannis et al., Cross-section measurements of capture reactions relevant to the p process using a $4\pi\gamma$-summing method. Phys. Rev. C **76**, 015802 (2007). https://doi.org/10.1103/PhysRevC.76.015802
9. A. Simon, S.J. Quinn, A. Spyrou et al., SuN: Summing NaI(Tl) gamma-ray detector for capture reaction measurements. Nucl. Instrum. Methods Phys. Res., Sect. A **703**, 16–21 (2013). https://doi.org/10.1016/j.nima.2012.11.045
10. C.S. Reingold, O. Olivas-Gomez, A. Simon et al., High efficiency total absorption spectrometer hector for capture reaction measurements. Eur. Phys. A **55**, 77 (2019). https://doi.org/10.1140/epja/i2019-12748-8
11. A.C. Dombos, D. Robertson, A. Simon et al., Measurement of low-energy resonance strengths in the $^{18}O(\alpha,\gamma)^{22}Ne$ reaction. Phys. Rev. Lett. **128**, 162701 (2022). https://doi.org/10.1103/PhysRevLett.128.162701
12. C. Casella, H. Costantini, A. Lemut et al., A new setup for the underground study of capture reactions. Nucl. Instrum. Methods Phys. Res., Sect. A **489**, 160–169 (2002). https://doi.org/10.1016/S0168-9002(02)00577-6
13. J. Su, H. Zhang, Z.H. Li et al., First result from the Jinping underground nuclear astrophysics experiment JUNA: precise measurement of the 92 keV $^{25}Mg(p,\gamma)^{26}Al$ resonance. Sci. Bull. **67**, 125–132 (2022). https://doi.org/10.1016/j.scib.2021.10.018
14. G.C. Yang, L.M. Hua, F. Lu et al., Response functions of a 4π summing gamma detector in β-Oslo method. Nucl. Sci. Tech. **33**, 68 (2022). https://doi.org/10.1007/s41365-022-01058-2
15. A. Sauerwein, H.-W. Becker, H. Dombrowski et al., Determination of $^{141}Pr(\alpha,n)^{144}Pm$ cross sections at energies of relevance for the astrophysical *p* process using the $\gamma\gamma$ coincidence method. Phys. Rev. C **84**, 045808 (2011). https://doi.org/10.1103/PhysRevC.84.045808
16. C.L. Jiang, K.E. Rehm, X. Fang et al., Measurements of fusion cross-sections in $^{12}C+^{12}C$ at low beam energies using a particle-γ coincidence technique. Nucl. Instrum. Methods Phys. Res., Sect. A **682**, 12–15 (2012). https://doi.org/10.1016/j.nima.2012.03.051
17. V.A.B. Zagatto, J.R.B. Oliveira, P.R.P. Allegro et al., γ-Particle coincidence technique for the study of nuclear reactions. Nucl. Instrum. Methods Phys. Res., Sect. A **749**, 19–26 (2014). https://doi.org/10.1016/j.nima.2014.02.014
18. R. Plag, M. Heil, F. Käppeler et al., An independent measurement of the $^{12}C(\alpha,\gamma)^{16}O$ cross section with the Karlsruhe 4π BaF_2 detector. Nucl. Phys. A **758**, 415–418 (2005). https://doi.org/10.1016/j.nuclphysa.2005.05.076
19. A.B. Zylstra, H.W. Hereman, Y.H. Kim et al., $^2H(p,\gamma)^3He$ cross section measurement using high-energy-density plasmas. Phys. Rev. C **101**, 042802 (2020). https://doi.org/10.1103/PhysRevC.101.042802
20. W.Z. Wang, C. Lv, X.P. Zhang et al., First measurement of the $^7Li(D,n)$ astrophysical S-factor in laser-induced full plasma. Phys. Lett. B **843**, 138034 (2023). https://doi.org/10.1016/j.physletb.2023.138034
21. H. Costantini, A. Formicola, G. Imbriani et al., LUNA: a laboratory for underground nuclear astrophysics. Rep. Prog. Phys. **72**, 086301 (2009). https://doi.org/10.1088/0034-4885/72/8/086301
22. W.P. Liu, Z.H. Li, J.J. He et al., Progress of Jinping underground laboratory for nuclear astrophysics (JUNA). Sci. China Phys. Mech. Astron. **59**, 642001 (2016). https://doi.org/10.1007/s11433-016-5785-9
23. T. Kajino, Underground laboratory JUNA shedding light on stellar nucleosynthesis. Nucl. Sci. Tech. **34**, 42 (2023). https://doi.org/10.1007/s41365-023-01196-1
24. W.P. Liu, B. Guo, Z. An et al., Recent progress in nuclear astrophysics research and its astrophysical implications at the China institute of atomic energy. Nucl. Sci. Tech. **35**, 217 (2024). https://doi.org/10.1007/s41365-024-01590-3
25. D. Robertson, M. Couder, U. Greife et al., Underground nuclear astrophysics studies with CASPAR. EPJ Web Conf. **109**, 09002 (2016). https://doi.org/10.1051/epjconf/201610909002
26. L.Y. Zhang, J. Su, J.J. He et al., Direct measurement of the astrophysical $^{19}F(p,\alpha\gamma)^{16}O$ reaction in the deepest operational underground laboratory. Phys. Rev. Lett. **127**, 152702 (2021). https://doi.org/10.1103/PhysRevLett.127.152702
27. L.Y. Zhang, J.J. He, R.J. deBoer et al., Measurement of $^{19}F(p,\gamma)^{20}Ne$ reaction suggests CNO breakout in first stars. Nature **610**, 656–660 (2022). https://doi.org/10.1038/s41586-022-05230-x
28. C. Ananna, F. Barile, A. Boeltzig et al., Underground measurements of nuclear reaction cross-sections relevant to AGB stars. Universe **8**, 4 (2022). https://doi.org/10.3390/universe8010004
29. L.H. Wang, J. Su, Y.P. Shen et al., Measurement of the $^{18}O(\alpha,\gamma)^{22}Ne$ reaction rate at JUNA and its impact on probing the origin of SiC grains. Phys. Rev. Lett. **130**, 092701 (2023). https://doi.org/10.1103/PhysRevLett.130.092701
30. H. Zhang, J. Su, Z.H. Li et al., Updated reaction rate of $^{25}Mg(p,\gamma)^{26}Al$ and its astrophysical implication. Phys. Rev. C **107**, 065801 (2023). https://doi.org/10.1103/PhysRevC.107.065801
31. R.M. Gesuè, G.F. Ciani, D. Piatti et al., First direct measurement of the 64.5 keV resonance strength in the $^{17}O(p,\gamma)^{18}F$ reaction. Phys. Rev. Lett. **133**, 052701 (2024). https://doi.org/10.1103/PhysRevLett.133.052701
32. Y.J. Chen, L.Y. Zhang, Examining the fluorine overabundance problem by conducting Jinping deep underground experiment. Nucl. Tech. **46**, 110501 (2023). https://doi.org/10.11889/j.0253-3219.2023.hjs.46.110501
33. Y.J. Chen, H. Zhang, L.Y. Zhang et al., Direct measurement of the break-out $^{19}F(p,\gamma)^{20}Ne$ reaction in the China Jinping underground laboratory (CJPL). Nucl. Sci. Tech. **35**, 143 (2024). https://doi.org/10.1007/s41365-024-01531-0
34. M. Aliotta, A. Boeltzig, R. Depalo et al., Exploring stars in underground laboratories: challenges and solutions. Annu. Rev. Nucl. Part. Sci. **72**, 177–204 (2022). https://doi.org/10.1146/annurev-nucl-110221-103625
35. B. Acharya, M. Aliotta, A. B. balantekin et al., Solar fusion III: New data and theory for hydrogen-burning stars (2024), https://

doi.org/10.48550/arXiv.2405.06470, arXiv:2405.06470 [astroph.SR]
36. R.C. Runkle, A.E. Champagne, C. Angulo et al., Direct measurement Fo the $^{14}N(p,\gamma)^{15}O$ S factor. Phys. Rev. Lett. **94**, 082503 (2005). https://doi.org/10.1103/PhysRevLett.94.082503
37. B. Frentz, A. Aprahamian, T. Borgwardt et al., Investigation of the $^{14}N(p,\gamma)^{15}O$ reaction and its impact on the CNO cycle. Phys. Rev. C **106**, 065803 (2022). https://doi.org/10.1103/PhysRevC.106.065803
38. K.-U. Kettner, H.W. Becker, C.R. Brune et al., Absolute cross section of the $^{12}C(p,\gamma)^{13}N$ reaction. Phys. Rev. C **108**, 035805 (2023). https://doi.org/10.1103/PhysRevC.108.035805
39. J.H. Li, Y.J. Li, Z.H. Li et al., Nuclear astrophysics research based on HI-13 tandem accelerator. Nucl. Tech. **46**, 080002 (2023). https://doi.org/10.11889/j.0253-3219.2023.hjs.46.080002
40. P. Jiao, Z.R. Hao, Q.K. Sun et al., Measurements of $^{27}Al(\gamma, n)$ reaction using quasi-monoenergetic γ beams from 13.2 to 21.7 MeV at SLEGS. Nucl. Sci. Tech. **36**, 66 (2025). https://doi.org/10.1007/s41365-025-01662-y
41. W.K. Nan, Y.B. Wang, Y.D. Sheng et al., Novel thick-target inverse kinematics method for the astrophysical $^{12}C+^{12}C$ fusion reaction. Nucl. Sci. Tech. **35**, 208 (2024). https://doi.org/10.1007/s41365-024-01573-4
42. P. Vojtyla, P.P. Povinec, Monte Carlo simulation of the muon-induced background of an anti-Compton gamma-ray spectrometer placed in a surface and underground laboratory. Radioact. Environ. **8**, 529–537 (2006). https://doi.org/10.1016/S1569-4860(05)08042-3
43. T. Szücs, D. Bemmerer, T.P. Reinhardt et al., Cosmic-ray-induced background intercomparison with actively shielded HPGe detectors at underground locations. Eur. Phys. J. A **51**, 33 (2015). https://doi.org/10.1140/epja/i2015-15033-0
44. T. Szücs, D. Bemmerer, D. Degering et al., Background in γ-ray detectors and carbon beam tests in the Felsenkeller shallow-underground accelerator laboratory. Eur. Phys. J. A **55**, 10 (2019). https://doi.org/10.1140/epja/i2019-12865-4
45. Y.D. Sheng, L.Y. Song, J. Su et al., The large-scale modular BGO detection array (LAMBDA) design and test. Nucl. Sci. Tech. **35**, 207 (2024). https://doi.org/10.1007/s41365-024-01574-3
46. S. Agostinelli, J. Allison, K. Amako et al., Geant4—a simulation toolkit. Nucl. Instrum. Methods Phys. Res., Sect. A **506**, 250 (2003). https://doi.org/10.1016/S0168-9002(03)01368-8
47. https://xia.com/support/pixie-16.html
48. X. PAN, Z.K. Lin, J.F. PAN, Experimental study and analysis of 5% boron-containing polyethylene shielded fast neutrons. Chin. J. Radiol. Health **22**, 396 (2013). https://doi.org/10.13491/j.cnki.issn.1004-714x.2013.04.001
49. Y.P. Shen, J. Su, W.P. Liu et al., Measurement of γ detector backgrounds in the energy range of 3–8 MeV at Jinping underground laboratory for nuclear astrophysics. Sci. China-Phys. Mech. Astron. **60**, 102022 (2017). https://doi.org/10.1007/s11433-017-9049-3
50. L. Zhao, W.T. Luo, B.P. Lar et al., Measurement of muon-induced neutron yield at the China Jinping underground laboratory. Chin. Phys. C **46**, 085001 (2022). https://doi.org/10.1088/1674-1137/ac66cc
51. J. Skowronski, R.M. Gesuè, A. Boeltzig et al., Advances in radiative capture studies at LUNA with a segmented BGO detector. J. Phys. G **50**, 045201 (2023). https://doi.org/10.1088/1361-6471/acb961
52. D.F. Hebbard, Proton capture by ^{15}N. Nucl. Phys. **15**, 289–315 (1960). https://doi.org/10.1016/0029-5582(60)90308-4
53. C. Rolfs, W.S. Rodney, Proton capture by ^{15}N at stellar energies. Nucl. Phys. A **235**, 450–459 (1974). https://doi.org/10.1016/0375-9474(74)90205-X
54. D. Bemmerer, C. Antonio et al., Direct measurement of the $^{15}N(p,\gamma)^{16}O$ total cross section at novae energies. J. Phys. G: Nucl. Part. Phys. **36**, 045202 (2009). https://doi.org/10.1088/0954-3899/36/4/045202
55. P.J. LeBlanc, I. Gianluca et al., Constraining the S factor of $^{15}N(p,\gamma)^{16}O$ at astrophysical energies. Phys. Rev. C **82**, 055804 (2010). https://doi.org/10.1103/PhysRevC.82.055804
56. A. Caciolli, C. Mazzocchi, V. Capogrosso et al., Revision of the $^{15}N(p,\gamma)^{16}O$ reaction rate and oxygen abundance in H-burning zones. Astron. Astrophys. **533**, A66 (2011). https://doi.org/10.1051/0004-6361/201117475
57. Y. Xu, K. Takahashi, S. Goriely et al., NACRE II: an update of the NACRE compilation of charged-particle-induced thermonuclear reaction rates for nuclei with mass number A<16. Nucl. Phys. A **918**, 61–169 (2013). https://doi.org/10.1016/j.nuclphysa.2013.09.007